PCCP

PAPER

View Article Online
View Journal | View Issue

Cite this: *Phys. Chem. Chem. Phys.*, 2022, **24**, 21853

Textural control of ionosilicas by ionic liquid templating†

Nicole Abdou,[a] Philippe Dieudonné-George,[b] Nicolas Brun, [a] Ahmad Mehdi *[a] and Peter Hesemann *[a]

Due to their unique self-assembly properties, ionic liquids (ILs) are versatile soft templates for the formation of mesoporous materials. Here, we report the use of ionic liquids as soft templates for the straightforward formation of mesoporous ionosilica phases. Ionosilicas are highly polyvalent functional materials that are constituted of ionic building blocks that are covalently immobilized within a silica hybrid matrix. Ionosilicas have attracted significant interest in the last few years due to their high potential for applications in water treatment and upgrading, separation and drug delivery. The straightforward and reproducible formation of mesoporous ionosilica phases is therefore highly desirable. In this context, we report the formation of mesoporous ionosilica phases *via* non-hydrolytic sol–gel procedures in the presence of ionic liquids. Ionic liquids appear as particularly versatile templates for mesoporous ionosilicas due to their high chemical similarity and affinity between ILs and silylated ionic precursors. We therefore studied the textures of the resulting ionosilica phases, after IL elimination, using nitrogen sorption, small angle X-ray scattering (SAXS) and transmission and scanning electron microscopies. All these techniques give concordant results and show that the textures of ionosilica scaffolds in terms of specific surface area, pore size, pore size distribution and connectivity can be efficiently controlled by the nature and the quantity of the ionic liquid that is used in the ionothermal sol–gel procedure.

Received 3rd June 2022,
Accepted 19th August 2022

DOI: 10.1039/d2cp02524h

rsc.li/pccp

Introduction

Ionic liquids (ILs) have been widely investigated over the last few decades for their unique properties such as high ionic conductivity and chemical stability, low vapor pressure and low flammability. ILs are salts with a melting point below 100 °C.[1] They are known as ''designer solvents'' since one can tailor their properties choosing a distinct cation/anion combination that matches the requirements of a given application. ILs with specific properties have been developed for applications in various domains such as energy storage,[2,3] catalysis,[4,5] gas adsorption,[6] *etc.* Besides, ILs, and in particular imidazolium based ILs, show a very particular self-organization behavior.[7–10] On one side, ILs form structured phases in the liquid state *via* the formation of extended hydrogen bonded networks.[11] On the other side, IL phases display nanoscale segregation in polar and non-polar domains.[12] The more pronounced this segregation is the longer the alkyl chain of the IL is. ILs therefore display heterogeneities at the nanoscopic level that linearly scale with the length of the alkyl chain.[12] The nanoscale segregation increases with the length of the alkyl chain, resulting in liquid-crystalline (LC) behavior for long chain substituted ILs.[13] Besides the length of the alkyl chain, the nature of the counter anion is also of prime importance for the formation of ionic liquid crystal phases. Whereas long-chain (>C12) substituted imidazolium halides form LC-phases, the corresponding bis-triflimides do not.[14,15] Altogether, ILs display a unique self-aggregation behavior at various levels, which results from their ability to form H-bonded networks, nanoscale segregation in polar/non-polar domains or even highly organized and ordered lyotropic phases.[16] Due to all these features, ILs should therefore be considered as 'supramolecular' solvents.[17]

This unique self-organizing behavior makes ILs efficient soft templates for the synthesis of mesoporous materials. Following the IUPAC nomenclature, mesoporous materials are porous compounds with a pore size between 2 and 50 nm[18] that display some interesting properties such as a high specific surface area and high pore volume. These features ensure enhanced diffusivity of large molecules throughout the material, with diffusion being the dominant mass transport mechanism in mesopores.[19] Due to their textural features including a high specific surface area, tunable pore size and high pore volume, mesoporous materials are potentially

[a] *ICGM, Univ Montpellier, CNRS, ENSCM, Montpellier, France. E-mail: peter.hesemann@umontpellier.fr*
[b] *Laboratoire Charles Coulomb (L2C), UMR 5221 CNRS-Univ Montpellier, France*

† Electronic supplementary information (ESI) available: Supplementary nitrogen sorption isotherms, BJH adsorption pore distribution, and supplementary SAXS diffractograms. See DOI: https://doi.org/10.1039/d2cp02524h

advantageous for applications in catalysis,[20] separation and energy storage.[21]

The first example of a mesoporous material synthesized in the presence of ILs goes back to the work of Dai *et al.* who reported the formation of a silica aerogel following a non-hydrolytic ionothermal sol–gel procedure.[22] Several years later, Antonietti *et al.* reported the synthesis of mesoporous silica using the IL $[C_4MIM]BF_4$. The elimination of the confined IL from the host matrix *via* washing led to a mesoporous silica material displaying a worm-like architecture.[23] The authors postulated a cooperative hydrogen bonding–π–π stacking mechanism to be responsible for the generation of mesoporosity and the formation of moderately ordered phases within this material. Finally, long-chain substituted imidazolium salts were used for their lyotropic properties. These compounds have successfully been used in hydrolysis polycondensation processes following classical templating strategies.[24,25]

The alkyl chain length of an IL has indeed a significant impact on the segregation in nano-domains within the IL and therefore also on the template effect in ionosilica synthesis. We consider that silica or ionosilica precursors, as polar components, have particular affinities toward the polar nano-domains of an IL, and that the non-polar domains particularly contribute to the formation of the texture of the materials. The size of the alkyl groups of an IL therefore has a direct influence on the textures of the materials formed in the presence of IL phases.[26,27]

These examples highlight the templating behavior of ILs and clearly indicate that the structuration of ILs can be transcribed to solid phases. ILs are therefore not only structured but also structuring phases, with high potential in the area of materials chemistry and in particular for the elaboration of materials *via* bottom-up approaches.[28–32]

Since several years, our special concern has been the elaboration of ionosilica phases with particular morphologies and architectures. We define ionosilicas as silica hybrid materials that are constituted of ionic building blocks.[33] Ionosilicas are highly modulable functional materials featuring a large range of surface and interface properties.[34,35] They found applications in water treatment and upgrading,[36,37] separation[38,39] and drug delivery.[40–42] Due to the high chemical similarity between ionosilicas and ILs and with the aim of studying the confinement of ILs within an ionosilica matrix, we recently focused on the formation of nanocomposites *via* hydrolysis–polycondensation reactions of ionosilica precursors in the presence of ILs.[43] For this purpose, we synthesized various ionosilica ionogels, and we could demonstrate particular confinement effects between the ionic host and guest. More specifically, we were able to show that an IL confined within an ionic host matrix forms two distinct populations: (i) the first one interacting with the pore walls *via* electrostatic interactions and (ii) the second one forming bulk-like IL domains.[44,45] As a particularity of these all-ionic composites, we could access free-standing and mechanically robust ionosilica ionogel monoliths containing up to 80 wt% of ILs by this approach which can be explained by the high affinity between the ionic host and the guest.

However, a systematic study of the textural properties of ionosilica scaffolds formed in the presence of ILs is missing so far. That is why we describe here how the textural properties of ionosilica scaffolds can be tuned as a function of the IL, *i.e. via* the amount of the used imidazolium bis-triflimide IL and the length of its cation alkyl chain. We demonstrate that ILs allow an efficient control of the texture of ionosilicas in terms of specific surface area, pore size and pore volume.

Experimental section

Chemicals

The ionosilica precursor tris(3-(trimethoxysilyl)propyl)amine (TTA) was synthesized following previously described protocols.[33] All imidazolium-based ionic liquids $[C_xMIM]TFSI$ (x = 2, 4, 6, 8, 12 and 16) were purchased from IoLiTec. Formic acid (p.a.) was purchased from VWR. All chemicals were used as received.

Synthesis of ionosilica materials

The synthesis of various ionosilica ionogels was performed in one-pot synthesis involving the ionosilica precursor **TTA**, formic acid and ionic liquid. Various imidazolium TFSI ILs with variable alkyl chain lengths were used: $[C_xMIM]TFSI$ (x = 2, 4, 6, 8, 12 and 16). The ionosilica matrices were formed *via* a non-hydrolytic sol–gel procedure from the tris(3-(trimethoxysilyl) propyl) amine precursor **TTA** in the presence of the IL. First, 3.0 g of the **TTA** precursor was mixed and vigorously stirred for three minutes with various molar amounts of IL in a Pyrex glass tube using a vortex apparatus. Then the polycondensation reaction was initiated by adding 2.0 mL of formic acid to the mixture. The exact quantities of the reactants in the ionosilica synthesis are given in Table 1. Gelation results from the transesterification–polycondensation reactions undergone by the trimethoxysilyl groups of the TTA precursor. Note that the protonation of the precursor occurs during the sol–gel process yielding the ionic building blocks of the ionosilica matrix. Colorless monoliths were obtained after 24 h at room temperature and kept under static conditions at 80 °C overnight. The ionosilica monoliths were obtained after the extraction of the IL with ethanol using a Soxhlet apparatus. Finally, the materials were dried at 80 °C under vacuum (0.01 mbar) for 24 h. The ionosilica monoliths were labelled as $TS_z^{C_x}$, where C_x is the length of the cation alkyl chain (x = 2, 4, 6, 8, 12, and 16) and z is the quantity of IL in mmoles.

Nitrogen sorption. Isotherms were recorded at 77 K using a Micromeritics TriStar volumetric apparatus by adding doses of N_2 in a measurement cell after an outgassing treatment of the

Table 1 Used quantities for the synthesis of ionosilica ionogel materials

	TTA		$[C_xMIM]TFSI$	HCOOH
	m (g)	n (mmol)	n (mmol)	V (mL)
$TS_3^{C_x}$	3.0	6.0	3.0	2.0
$TS_{10}^{C_x}$	3.0	6.0	10.0	2.0
$TS_{20}^{C_x}$	3.0	6.0	20.0	2.0
$TS_{41}^{C_x}$	3.0	6.0	41.0	2.0

samples at 120 °C under vacuum overnight. The BET surface area of each sample was determined using the Brunauer–Emmett–Teller (BET) method[46] in the linear range of the isotherms typically at p/p_0 = 0.05–0.15. The pore size distribution was calculated using the Barret–Joyner–Halenda (BJH) method[47] from the adsorption isotherm. The total pore volume of the materials was determined at p/p_0 = 0.99.

Small angle X-ray scattering (SAXS). Experiments were performed using an in-house setup of the Laboratoire Charles Coulomb, Université de Montpellier, France. A high brightness low power X-ray tube, coupled with an aspheric multilayer optic (GeniX^{3D} from Xenocs), was employed. It delivers an ultralow divergent beam (0.5 mrad, λ = 0.15418 nm). Scatterless slits were used to give a clean 0.6 mm beam diameter with a flux of 35 Mphotons s^{-1}. We worked in a transmission configuration where the scattered intensity was measured using a 2D "Pilatus" 300 K pixel and detected using a Dectris detector (490 × 600 pixels) with a pixel size of 172 × 172 μm^2, placed at a 1.9 m distance from the sample. All intensities were corrected by transmission and the empty cell contribution (glass capillary) was subtracted.

Transmission electron microscopy (TEM). TEM measurements were performed with a FEG JEOL 2200 FS-200 KV electron microscope equipped with a CCD GATAN USC camera with 4092 × 4092 pixels and an electron gun of 200 kV. The probe diameter in STEM mode is about 1 nm with a resolution of up to 0.1 nm.

Scanning electron microscopy (SEM). Images were taken using a Hitachi S-4800 microscope, Japan. A 2 kV acceleration voltage was applied on the ground IL free samples.

Results and discussion

Nonhydrolytic sol–gel reactions of silylated precursors in the presence of ionic liquids result in the formation of silica based ionogels, where an ionic liquid is trapped within a silica matrix.[22] Following this strategy, we recently reported ionosilica ionogels, a special case of all-ionic composite materials,[43] formed from ionosilica precursors. Although the confinement of the IL was investigated and strong interactions between the ionic host and guest could be demonstrated, the texture of the formed ionosilica scaffolds that are formed in this non-hydrolytic sol–gel approach has not been investigated so far. In this work, we therefore focused on the characteristics of the ionosilica scaffolds formed using the non-hydrolytic sol–gel approach, obtained after IL elimination by washing. We determined in particular the textural characteristics of the ionosilicas as a function of the reaction parameters, in particular of the quantity and the constitution of the used IL. We investigated the characteristics of the ionosilica materials as a function of two parameters: (1) the amount of ILs [C$_x$MIM]TFSI in the hydrolysis–polycondensation mixture and (2) the length of the alkyl chain on the imidazolium cation.

More specifically, the ionosilica materials were obtained from the tris-trialkoxysilylated amine precursor **TTA** (Fig. 1a) in the presence of various methyl-alkylimidazolium bis-triflimides (Fig. 1b) *via* non-hydrolytic sol–gel reactions in the presence of formic acid.[48] Ionosilica ionogel monoliths are formed at room temperature after several hours. After aging at 80 °C and IL elimination by washing, we obtained ionosilica phases that are labelled as $TS_z^{C_x}$, where z is the quantity of the IL in mmoles and C_x is the length of the cation alkyl chain (x = 2, 4, 6, 8, 12 and 16). Here, we focused particularly on the impact of two parameters on the texture of the formed ionosilicas: (i) the quantity of the IL and (ii) the length of the alkyl chain of the methyl–alkyl imidazolium cation, and we studied the textural properties of the obtained materials *via* nitrogen sorption, small-angle X-ray scattering (SAXS), and scanning and transmission electron microscopies (SEM and TEM).

Nitrogen sorption measurements at 77 K allowed determining the textural properties of the materials in terms of specific surface area, S_{BET}, pore volume, V_p, and pore size, D_p. The results are summarized in Table 2, and a histogram of the specific surface area data of the materials is shown in Fig. 2. Histograms displaying the pore sizes and pore volumes are given in the ESI† (Fig. S1 and S2).

At a first glance, the formed monoliths are moderately to highly porous materials, with specific surface areas in the range of 300–600 m^2 g^{-1}. The materials are mostly mesoporous with pore diameters in the range of 25–55 Å, except those that are synthesized with the lowest amount of IL, *i.e.*, the $TS_3^{C_x}$ series obtained with 3 mmoles of the IL. These latter materials are non-porous with specific surface areas S_{BET} < 1 m^2 g^{-1}. It should be mentioned that all $TS_z^{C_x}$ materials (z = 10, 20 and 41) display a large pore size distribution (Fig. S3–S8, ESI†).

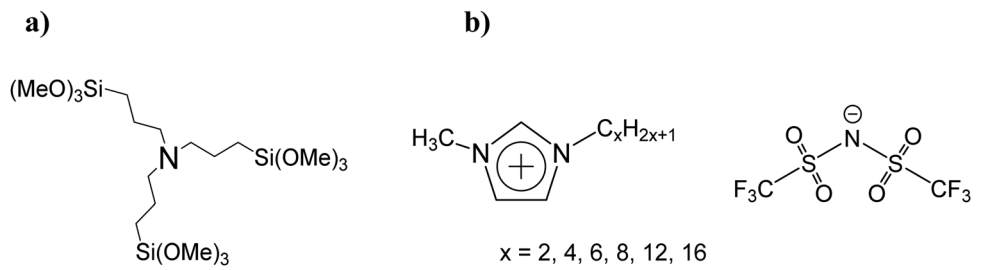

Fig. 1 (a) Molecular structure of the ionosilica precursor tris(3-(trimethoxysilyl)propyl)amine (**TTA**). (b) Molecular structure of the used imidazolium-based ionic liquids [C$_x$MIM]TFSI.

Table 2 BET surface areas, pore volumes and pore diameters of ionosilica monoliths synthesized in the presence of [C_xMIM]TFSI ionic liquids. The sets of materials that are discussed in detail in the text are in bold

	S_{BET} (m^2 g^{-1})				Total pore volume V_p[a] (cm^3 g^{-1})				Pore diameter D_p[b] (Å)			
z (mmol)	3	10	**20**	41	3	10	**20**	41	3	10	**20**	41
$TS_z^{C_2}$	<1	76	**444**	358	n.d.	0.04	**0.31**	0.31	n.d.	23	**30**	36
$TS_z^{C_4}$	**<1**	**310**	**463**	**306**	**n.d.**	**0.17**	**0.35**	**0.30**	**n.d.**	**24**	**31**	**34**
$TS_z^{C_6}$	<1	306	**463**	353	n.d.	0.16	**0.36**	0.30	n.d.	24	**32**	35
$TS_z^{C_8}$	<1	402	**525**	500	n.d.	0.22	**0.52**	0.50	n.d.	25	**39**	39
$TS_z^{C_{12}}$	<1	516	**577**	520	n.d.	0.39	**0.81**	0.70	n.d.	32	**55**	52
$TS_z^{C_{16}}$	356	520	**600**	590	0.22	0.50	**0.78**	0.77	27	34	**52**	50

[a] Determined at p/p_0 0.99. [b] Calculated following the Harkins and Jura equation.[49]

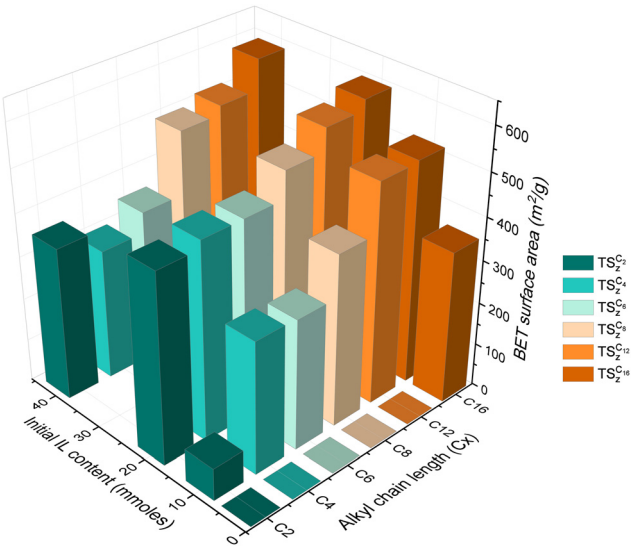

Fig. 2 Histograms of the BET surface areas of the IL-free ionosilica ionogels $TS_z^{C_x}$, synthesized in the presence of different volumes of imidazolium ILs [C_xMIM]TFSI (x = 2, 4, 6, 8, 12 and 16).

In order to highlight the impact of the two investigated parameters, *i.e.*, the quantity of the IL and the substitution of the alkyl chain of the methyl–alkyl imidazolium cation, on the textures and architectures of the formed ionosilica phases, we discuss more in detail two sets of materials:

(i) The ionosilicas, $TS_z^{C_4}$, synthesized in the presence of variable amounts of the IL [C_4MIM]TFSI on the one side and.

(ii) The ionosilicas, $TS_{20}^{C_x}$, synthesized in the presence of 20 mmoles of different methyl–alkylimidazolium bis-triflimides with different alkyl chain lengths on the other side. The nitrogen sorption isotherms of both series of materials are shown in Fig. 3a and b.

In the series of ionosilicas, $TS_z^{C_4}$, formed in the presence of variable amounts of [C_4MIM]TFSI, our results indicate the low porosity of the material $TS_3^{C_4}$ that is synthesized in the presence of the lowest quantity of the IL (3 mmoles). For the materials $TS_{10}^{C_4}$ and $TS_{20}^{C_4}$, a significant increase of the specific surface area was observed, to reach a maximum value for the material $TS_{20}^{C_4}$. Finally, the material *c*, synthesized in the presence of the highest quantity of the IL, shows a slightly lower specific surface area compared to material $TS_{20}^{C_4}$. This general trend can be found in all other series of ILs, synthesized in the presence of variable amounts of a given IL.

The evolution of the pore volume in the series of the materials $TS_z^{C_4}$ follows an identical trend. We found increasing values up to the material $TS_{20}^{C_4}$. This material shows the highest pore volume in this series. The pore volume slightly decreased when the IL quantity is further increased, *i.e.*, in the case of the material $TS_{41}^{C_4}$.

In contrast, the pore diameter progressively increases in this series of materials. This evolution can clearly be seen in the nitrogen sorption *via* the shape of the isotherms (Fig. 3a). Material $TS_3^{C_4}$ displays low porosity, whereas the material $TS_{10}^{C_4}$ gives rise to a type I isotherm, evidencing the presence of supermicropores (wide micropores of widths between 7 and 20 Å). The materials $TS_{20}^{C_4}$ and $TS_{41}^{C_4}$ show type IV isotherms with H2(a) type hysteresis loops, confirming the presence of narrow mesopores with diameters of 30 and 35 Å, respectively. The very steep decrease in the desorption branch at a relative pressure of *ca.* 0.4 is typical of cavitation-induced evaporation (the pore body empties while the pore neck remains filled) and suggests the presence of bottle-neck type mesopores.[50]

Regarding the series of materials $TS_{20}^{C_x}$, synthesized in the presence of 20 mmoles of methyl-alkylimidazolium bis-triflimides, we observed an increase of the specific surface area, pore size and pore diameter for the materials with ethyl, butyl, hexyl, octyl and dodecyl groups (Fig. 3b). The specific surface area levels off for the material $TS_{20}^{C_{16}}$. In contrast, whereas the use of short-chain substituted ILs (C_2–C_6) results in the formation of materials with similar pore sizes, the use of long-chain substituted ILs (C_{12}/C_{16}) led to materials with significantly larger pores, as indicated by the different shape of the nitrogen sorption isotherms (Fig. 3b and Table 2 – pore diameter). This latter result indicates a particular templating behavior of long chain substituted ILs, namely of dodecyl- and hexadecyl-methylimidazolium bis-triflimide.

Our results therefore reveal a clear correlation between the nature and the amount of the IL on the textures of the formed materials. They indicate that the supramolecular aggregation of imidazolium based bis-triflimide ILs in hydrophilic and hydrophobic domains has a direct impact on the texture of the formed ionosilicas in terms of the specific surface area, pore size and pore volume. The porosity of the ionosilica matrix can be well tuned both *via* the amount of the confined IL and the length of the cation alkyl chain.

We then performed small angle X-ray scattering (SAXS) in order to obtain a more detailed insight into the pore architecture of the materials. Similar to the results of nitrogen sorption experiments, we discuss here more in detail the same sets of materials: (i) the ionosilicas $TS_z^{C_4}$, synthesized in the presence of variable quantities of the IL [C_4MIM]TFSI on the one side

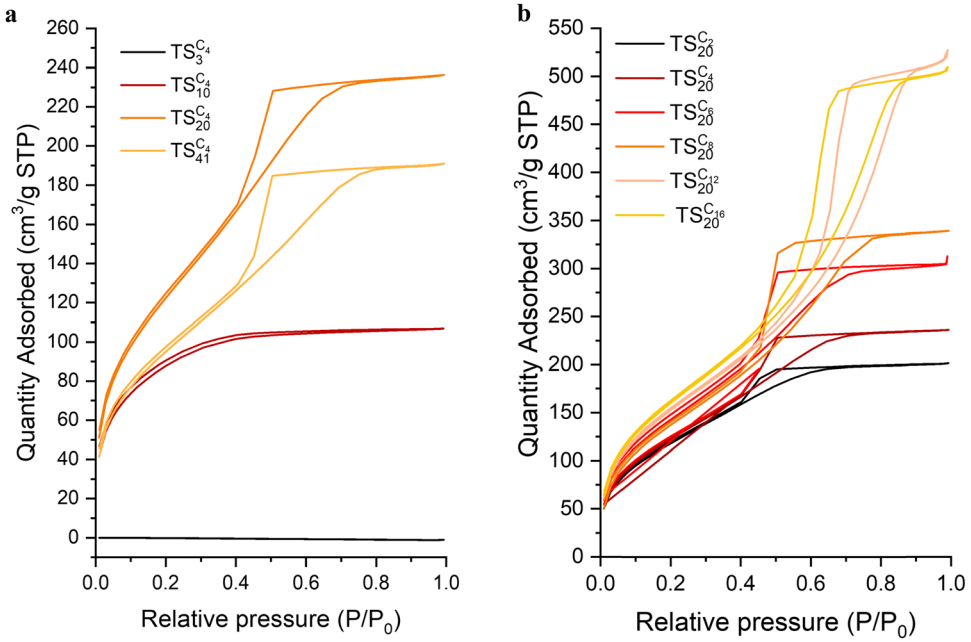

Fig. 3 (a) Nitrogen sorption isotherms of monoliths synthesized in the presence of variable amounts of [C_4MIM]TFSI. (b) Nitrogen sorption isotherms of the ionosilica monoliths synthesized in the presence of 20 mmoles of methyl-alkylimidazolium bis-triflimides [C_xMIM]TFSI with variable alkyl chain lengths (x = 2, 4, 6, 8, 12 and 16).

and (ii) the ionosilicas $TS_{20}^{C_x}$, synthesized in the presence of 20 mmoles of different methyl-alkylimidazolium bis-triflimides with different alkyl chain lengths on the other side. The SAXS patterns of the $TS_z^{C_4}$ materials are shown in Fig. 4, and the patterns of the series $TS_{20}^{C_x}$ are shown in Fig. S13 (ESI†).

Similar SAXS profiles were obtained for all the materials of the $TS_z^{C_4}$ series (Fig. 4), synthesized in the presence of different quantities of ILs. However, the patterns show some significant evolutions namely in the high q (q = ~0.5–1 nm^{-1}) and low q domains (q = ~0.15–0.4 nm^{-1}). For q values in the range of ~0.5–1 nm^{-1}, SAXS intensity profiles show a cross over, whose position clearly shifts toward lower q values as a function of the molar fraction z of the ionic liquid used to prepare the $TS_z^{C_x}$ samples.

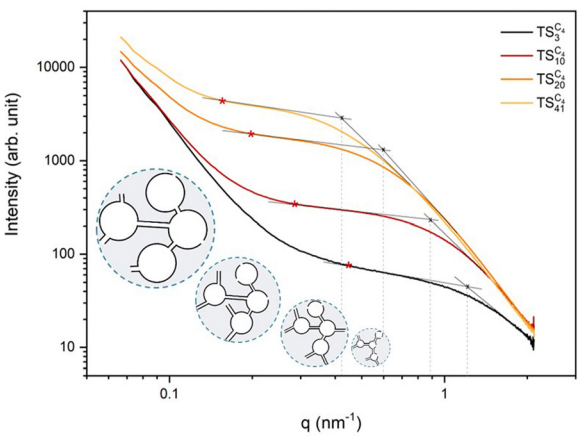

Fig. 4 SAXS patterns of the $TS_z^{C_4}$ monoliths synthesized in the presence of variable amounts of [C_4MIM]TFSI (z = 3, 10, 20 and 41).

This q region profile should be the characteristic of the form factor of pores in mesoporous solids. In the case of worm-like ink-bottle pores, we can estimate, from the q-position of the cross over (see dashed lines in Fig. 4), the order of magnitude of the average pore diameter d (nm) using the eqn (1):

$$d\ (\mathrm{nm}) \sim 2/q(\mathrm{nm}^{-1}) \quad (1)$$

The shift of the cross over toward lower q values as a function of z (Fig. 4), from 1.188 nm^{-1} for $TS_3^{C_4}$ to 0.420 nm^{-1} for $TS_{41}^{C_4}$, clearly indicates an increase of the pore diameter values obtained by SAXS, from ~17 to ~48 Å, respectively (Table 3). The increase in the quantity of [C_4MIM]TFSI therefore promotes the formation of larger confined ionic liquid domains within the host matrix, resulting in the formation of larger pores within the ionosilica scaffold after IL elimination. Interestingly, the values of the pore diameters obtained from nitrogen sorption and SAXS

Table 3 Small-angle X-ray scattering data of $TS_z^{C_x}$ monoliths with different ratios of [C_xMIM]TFSI ionic liquids

	Pore diameter[a] (Å)				Pore diameter[b] (Å)			
n (mmol)	3	10	***20***	41	3	10	***20***	41
$TS_z^{C_2}$	14	22	***34***	47	n.d.	23	***30***	36
$TS_z^{C_4}$	***17***	***22***	***33***	***48***	n.d.	***24***	***31***	***34***
$TS_z^{C_6}$	16	26	***35***	47	n.d.	24	***32***	35
$TS_z^{C_8}$	19	24	***39***	49	n.d.	25	***39***	39
$TS_z^{C_{12}}$	n.d	n.d	***48***	n.d	n.d.	32	***55***	52
$TS_z^{C_{16}}$	n.d	n.d	***42***	n.d	27	34	***52***	50

[a] Determined by SAXS using relation (1). [b] Calculated using the Harkins and Jura equation from nitrogen sorption analysis.[49]

measurements are in good agreement (Table 3). The slightly higher values obtained by SAXS compared to those obtained by nitrogen sorption can be explained by limited pore filling in the case of closed porosity or interconnected pores with too narrow openings in nitrogen sorption experiments. Furthermore, some pores could also not be completely filled with nitrogen, depending on the pore surface curvature distribution (convex/concave).[51] Comparatively, the SAXS signal only depends on the real volumetric distribution of density fluctuations inside the monolith, regardless of the pore architecture and connectivity. Therefore, the pore sizes obtained by nitrogen sorption are then often underestimated compared to SAXS values, as also observed here.

At lower q values (in the $\sim$0.15–0.4 nm^{-1} q range), a second cross-over can be observed for all samples (Fig. 4). This type of SAXS profile suggests the aggregation of individual pores into primary pore clusters. Pores are interconnected by narrow paths to form larger pore domains in accordance with the "ink-bottle" shape deduced from the mentioned H2 type isotherms observed in Fig. 3a and b. Such primary porous clusters can be interconnected to form larger pore aggregates (at the 100–1000 nm scale), as suggested by the significant increase of the scattering intensity observed at lower q values as shown in Fig. 4 for all samples. A characteristic size d' (nm) of the primary clusters can also be deduced from relation (1). A shift toward lower q values of the primary cluster cross-over as a function of z is observed in Fig. 4. It can be seen that d' increases proportionally to the z value from $\sim$40 Å (TS_3^{Cx}) to $\sim$125 Å (TS_{41}^{Cx}) that corresponds to 2–3 times the size of the individual pore size.

Regarding the second series of materials TS_{20}^{Cx}, we also studied the effect of the length of the cation alkyl chain on the textural properties of the obtained material *via* SAXS measurements. As discussed earlier, the alkyl chains of the IL tend to aggregate into nonpolar domains whereas the imidazolium ring and the anion form polar domains.[52] The increase of the length of the alkyl chain of the cation is expected to enlarge the nonpolar IL domains.[15] The SAXS profiles (Fig. S13, ESI†) show the presence of two evolution domains as function of the length of the cation alkyl chain (C_x), similarly to the results discussed in Fig. 4 (*vide supra*). The average size of pores and pore primary-clusters clearly increases with the increase of the length of the cation alkyl chain for $x > 8$. SAXS experiments therefore indicate the same trend as observed in nitrogen sorption measurements and confirm that only the long-chain substituted imidazolium ILs (C12 and C16) led to an increase of the pore diameters, whereas no significant increase of the pore size could be observed for short chain substituted species ($C < 10$). These results therefore highlight a particular self-aggregation behavior of dodecyl- and hexadecyl-imidazolium bis-triflimides, as already described earlier.[53]

Finally, the morphologies and textures of the materials were studied *via* scanning and transmission electron microscopies (SEM and TEM). Fig. 5 shows the SEM images of the materials $TS_{20}^{C_2}$, $TS_{20}^{C_8}$ and $TS_{20}^{C_{16}}$, all synthesized in the presence of 20 mmoles of [C_xMIM]TFSI (x = 2, 8 and 16).

SEM images show that the materials consist of agglomerated primary particles of nanometric size (at the 10–100 nm scale). The diameter of the primary particles depends on the nature of the used ILs and increases with increasing alkyl chain length. Hence, the utilization of long chain (C_{16}) substituted imidazolium bis-triflimides led to the formation of a material displaying a widened architecture, larger pores and larger granulometry

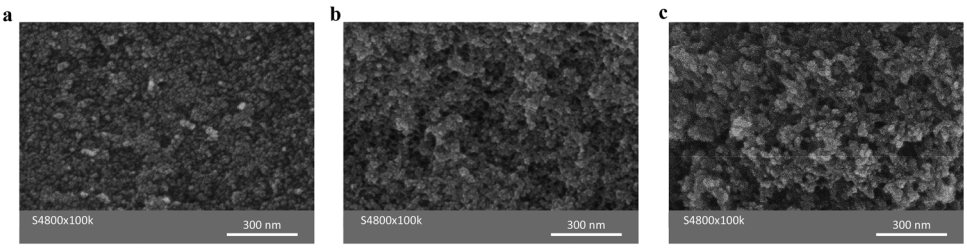

Fig. 5 Scanning electron microscopy (SEM) images of $TS_{20}^{C_2}$, $TS_{20}^{C_8}$ and $TS_{20}^{C_{16}}$ monoliths with 20 mmoles of (a) [C_2MIM]TFSI, (b) [C_8MIM]TFSI and (c) [C_{16}MIM]TFSI. Scale bar: 300 nm.

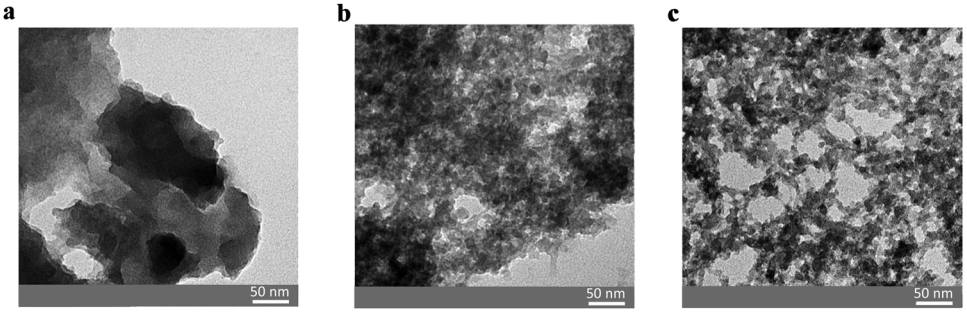

Fig. 6 Transmission electron microscopy (TEM) images of the materials $TS_{20}^{C_2}$, $TS_{20}^{C_8}$ and $TS_{20}^{C_{16}}$.

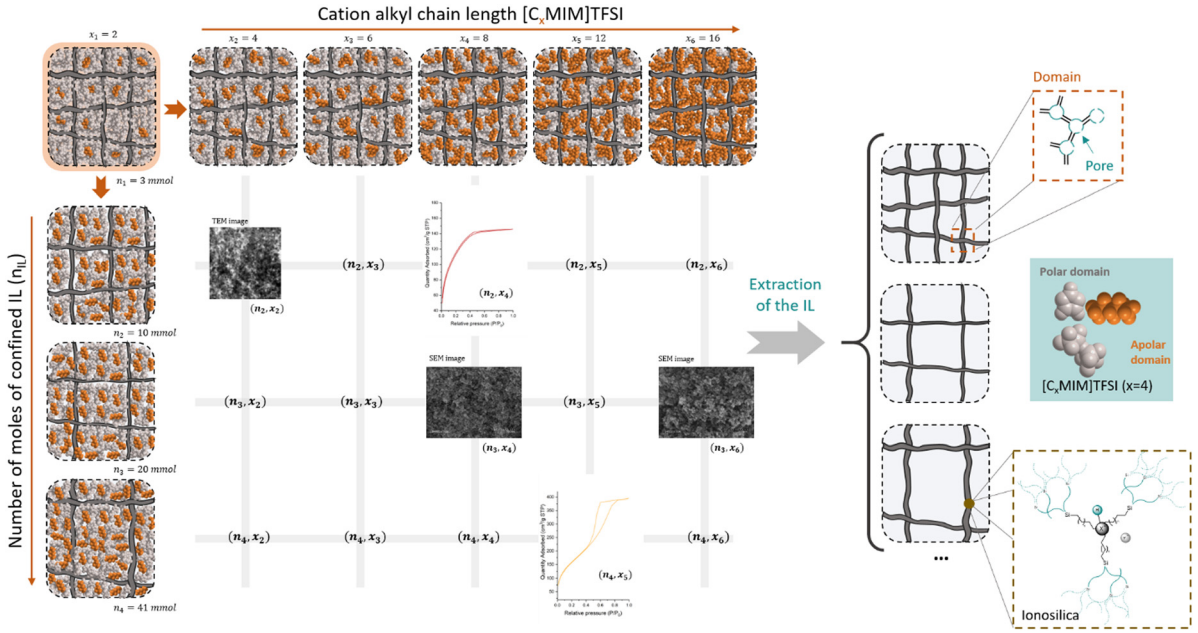

Fig. 7 Scheme resuming the mesoporosity control *via* the number of moles of the confined IL and the cation alkyl chain length.

compared to the two other materials as shown in Fig. 5(a–c). All formed ionosilicas show interconnected pore architectures ensuring good diffusion throughout the whole material. SEM images seem to reveal the existence of macropores that cannot be detected neither by gas sorption nor by SAXS techniques.

The texture of the materials was then observed by transmission electron microscopy (TEM). The TEM images of the materials $TS_{20}^{C_2}$, $TS_{20}^{C_8}$ and $TS_{20}^{C_{16}}$, all synthesized in the presence of 20 mmoles of [C$_x$MIM]TFSI (x = 2, 8 and 16), are displayed in Fig. 6.

TEM images of the materials also show that the nature of the used IL has a direct impact on the texture and directly affects the morphology of the formed materials. The TEM image of the material $TS_{20}^{C_2}$ shows a dense matrix indicating the presence of a low porous or mesoporous material (Fig. 6a), whereas the TEM images of $TS_{20}^{C_8}$ and $TS_{20}^{C_{16}}$ (Fig. 6b and c) reveal a macroporosity with increasing pore widths. These results confirm the meso–macroporous characteristics of these materials and an increase of both macropore and macropore sizes of the materials with the length of the cation alkyl chain of the ionic liquid. The interconnected macropores form pore domains of about 50 nm width for $TS_{20}^{C_{16}}$ (Fig. 6c).

To sum up, nitrogen sorption and SAXS measurements of the ionosilica materials give a complete and concordant image of the mesoporous textures and architectures (at the 1–10 nm scale) of the ionosilica materials formed in the presence of ionic liquids (Fig. 7). Both investigated parameters, the quantity of the IL used for the sol–gel procedure on the one side (Fig. 7 – *vertical*) and the alkyl chain length of the imidazolium cation on the other side (Fig. 7 – *horizontal*), contribute to the evolution of the texture and morphology of the formed ionosilica materials. The increase in the amount of the IL leads to an increase of the specific surface area and enlarged mesopore diameter and primary clusters within the ionosilica scaffold. On the other side, the increase of the alkyl chain length of the cation also contributes to increasing specific surface areas. However, a significant increase of the pore diameters could only be observed with long-chain substituted ILs, *i.e.*, imidazolium cations bearing dodecyl or hexadecyl groups. The texture of ionosilicas formed in non-hydrolytic sol–gel synthesis involving room-temperature ionic liquids can therefore efficiently be controlled by the two studied parameters.

Conclusion

We report ionosilica materials obtained *via* a non-hydrolytic sol–gel procedure in the presence of various methylalkylimidazolium bis-triflimide ILs. The aim was to study the effect of the amount of the confined IL and the length of its cation alkyl chain on the morphological and textural properties of the ionosilica scaffold after the extraction of the IL. This study clearly shows a clear correlation between both the investigated parameters and the textural properties of the ionosilica scaffold. It also reveals, for our ionosilica monoliths, the existence of both macroporosity and mesoporosity. Electron microscopy analyses indicate that the ionosilica scaffolds show a tunable interconnected macroporosity. Nitrogen sorption and SAXS measurements give concordant results and show that by increasing the quantity of a given IL, an increase of the mesoporosity in terms of the specific surface area, pore volume and pore diameter could be observed, with a maximum for the materials synthesized in the presence of 20 mmoles of IL. Regarding materials obtained in the presence of a specific amount of the IL [C$_x$MIM]TFSI bearing different alkyl chain

lengths (x = 2, 4, 6, 8, 12 and 16), an increase of the specific surface area could be detected. However, different substitution of the imidazolium cation leads to an increasing pore size only with long-chain substituted ILs ($C > 8$), thus highlighting a particular self-aggregation behavior of imidazolium bis-triflimides bearing dodecyl or hexadecyl groups. Our results indicate that the supramolecular aggregation of imidazolium based bis-triflimide ILs in hydrophilic and hydrophobic domains has a direct impact on the texture of the formed ionosilicas.

Author contributions

The manuscript was written through contributions of all the authors. All the authors gave approval to the final version of the manuscript.

Conflicts of interest

The authors declare no competing financial interest.

Acknowledgements

The authors are grateful for the excellent technical assistance of Didier Cot and Bertrand Rebière for SEM measurements and Franck Godiard for TEM measurements.

References

1 M. Salanne, L. J. A. Siqueira, A. P. Seitsonen, P. A. Madden and B. Kirchner, From molten salts to room temperature ionic liquids: simulation studies on chloroaluminate systems, *Faraday Discuss.*, 2012, **154**, 171–188.
2 M. Watanabe, M. L. Thomas, S. Zhang, K. Ueno, T. Yasuda and K. Dokko, Application of Ionic Liquids to Energy Storage and Conversion Materials and Devices, *Chem. Rev.*, 2017, **117**(10), 7190–7239.
3 A. Vioux and B. Coasne, From Ionogels to Biredox Ionic Liquids: Some Emerging Opportunities for Electrochemical Energy Storage and Conversion Devices, *Adv. Energy Mater.*, 2017, 7(22), 1700883.
4 V. I. Pârvulescu and C. Hardacre, Catalysis in Ionic Liquids, *Chem. Rev.*, 2007, **107**(6), 2615–2665.
5 J. P. Hallett and T. Welton, Room-Temperature Ionic Liquids: Solvents for Synthesis and Catalysis. 2, *Chem. Rev.*, 2011, **111**(5), 3508–3576.
6 M. Hasib-ur-Rahman, M. Siaj and F. Larachi, Ionic liquids for CO_2 capture—Development and progress, *Chem. Eng. Process.*, 2010, **49**(4), 313–322.
7 M. A. A. Rocha, C. Neves, M. G. Freire, O. Russina, A. Triolo, J. A. P. Coutinho and L. Santos, Alkylimidazolium Based Ionic Liquids: Impact of Cation Symmetry on Their Nanoscale Structural Organization, *J. Phys. Chem. B*, 2013, **117**(37), 10889–10897.
8 A. Triolo, O. Russina, B. Fazio, R. Triolo and E. Di Cola, Morphology of 1-alkyl-3-methylimidazolium hexafluorophosphate room temperature ionic liquids, *Chem. Phys. Lett.*, 2008, **457**(4–6), 362–365.
9 O. Russina, L. Gontrani, B. Fazio, D. Lombardo, A. Triolo and R. Caminiti, Selected chemical-physical properties and structural heterogeneities in 1-ethyl-3-methylimidazolium alkyl-sulfate room temperature ionic liquids, *Chem. Phys. Lett.*, 2010, **493**(4–6), 259–262.
10 O. Russina, A. Triolo, L. Gontrani, R. Caminiti, D. Xiao, L. G. Hines, R. A. Bartsch, E. L. Quitevis, N. Plechkova and K. R. Seddon, Morphology and intermolecular dynamics of 1-alkyl-3-methylimidazolium bis{(trifluoromethane)sulfonyl}-amide ionic liquids: structural and dynamic evidence of nanoscale segregation, *J. Phys.: Condens. Matter*, 2009, **21**, 424121.
11 S. Saha, S. Hayashi, A. Kobayashi and H. Hamaguchi, Crystal structure of 1-butyl-3-methylimidazolium chloride. A clue to the elucidation of the ionic liquid structure, *Chem. Lett.*, 2003, **32**(8), 740–741.
12 A. Triolo, O. Russina, H.-J. Bleif and E. Di Cola, Nanoscale Segregation in Room Temperature Ionic Liquids, *J. Phys. Chem. B*, 2007, **111**(18), 4641–4644.
13 Y. M. Ji, R. Shi, Y. T. Wang and G. Saielli, Effect of the Chain Length on the Structure of Ionic Liquids: from Spatial Heterogeneity to Ionic Liquid Crystals, *J. Phys. Chem. B*, 2013, **117**(4), 1104–1109.
14 A. E. Bradley, C. Hardacre, J. D. Holbrey, S. Johnston, S. E. J. McMath and M. Nieuwenhuyzen, Small-angle X-ray scattering studies of liquid crystalline 1-alkyl-3-methylimidazolium salts, *Chem. Mater.*, 2002, **14**(2), 629–635.
15 D. Pontoni, J. Haddad, M. Di Michiel and M. Deutsch, Self-segregated nanostructure in room temperature ionic liquids, *Soft Matter*, 2017, **13**(38), 6947–6955.
16 A. F. Bouarab, J. P. Harvey and C. Robelin, Viscosity models for ionic liquids and their mixtures, *Phys. Chem. Chem. Phys.*, 2021, **23**(2), 733–752.
17 M. Antonietti, D. B. Kuang, B. Smarsly and Z. Yong, Ionic liquids for the convenient synthesis of functional nanoparticles and other inorganic nanostructures, *Angew. Chem., Int. Ed.*, 2004, **43**(38), 4988–4992.
18 J. Rouquerol, D. Avnir, C. W. Fairbridge, D. H. Everett, J. H. Haynes, N. Pernicone, J. D. F. Ramsay, K. S. W. Sing and K. K. Unger, Recommendations for the Characterization of Porous Solids, *Pure Appl. Chem.*, 1994, **66**(8), 1739–1758.
19 B. Coasne, Multiscale adsorption and transport in hierarchical porous materials, *New J. Chem.*, 2016, **40**(5), 4078–4094.
20 N. Artioli, R. F. Lobo and E. Iglesia, Catalysis by Confinement: Enthalpic Stabilization of NO Oxidation Transition States by Microporous and Mesoporous Siliceous Materials, *J. Phys. Chem. C*, 2013, **117**(40), 20666–20674.
21 W. Li, J. Liu and D. Zhao, Mesoporous materials for energy conversion and storage devices, *Nat. Rev. Mater.*, 2016, **1**(6), 16023.
22 S. Dai, Y. H. Ju, H. J. Gao, J. S. Lin, S. J. Pennycook and C. E. Barnes, Preparation of silica aerogel using ionic liquids as solvents, *Chem. Commun.*, 2000, (3), 243–244.
23 Y. Zhou, J. H. Schattka and M. Antonietti, Room-Temperature Ionic Liquids as Template to Monolithic

Mesoporous Silica with Wormlike Pores via a Sol–Gel Nanocasting Technique, *Nano Lett.*, 2004, **4**(3), 477–481.

24 T. W. Wang, H. Kaper, M. Antonietti and B. Smarsly, Templating behavior of a long-chain ionic liquid in the hydrothermal synthesis of mesoporous silica, *Langmuir*, 2007, **23**(3), 1489–1495.

25 S. Vavra, N. Vilà, A. Lotsari, A. Walcarius and A. Martinelli, An imidazolium ionic liquid as effective structure-directing agent for the fabrication of silica thin films with vertically aligned nanochannels, *Microporous Mesoporous Mater.*, 2020, 110407.

26 A. Martinelli, Effects of a Protic Ionic Liquid on the Reaction Pathway during Non-Aqueous Sol-Gel Synthesis of Silica: A Raman Spectroscopic Investigation, *Int. J. Mol. Sci.*, 2014, **15**(4), 6488–6503.

27 M. Nayeri, K. Nygard, M. Karlsson, M. Marechal, M. Burghammer, M. Reynolds and A. Martinelli, The role of the ionic liquid C(6)C(1)ImTFSI in the sol–gel synthesis of silica studied using in situ SAXS and Raman spectroscopy, *Phys. Chem. Chem. Phys.*, 2015, **17**(15), 9841–9848.

28 Z. Ma, J. Yu and S. Dai, Preparation of Inorganic Materials Using Ionic Liquids, *Adv. Mater.*, 2010, **22**(2), 261–285.

29 C.-C. Han, S.-Y. Ho, Y.-P. Lin, Y.-C. Lai, W.-C. Liang and Y.-W. Chen-Yang, Effect of π–π stacking of water miscible ionic liquid template with different cation chain length and content on morphology of mesoporous TiO_2 prepared via sol–gel method and the applications, *Microporous Mesoporous Mater.*, 2010, **131**(1), 217–223.

30 K. Z. Donato, L. Matejka, R. S. Mauler and R. K. Donato, Recent Applications of Ionic Liquids in the Sol–Gel Process for Polymer-Silica Nanocomposites with Ionic Interfaces, *Colloids Interfaces*, 2017, **1**, 5.

31 N. Rameli, K. Jumbri, R. A. Wahab, A. Ramli and F. Huyop, Synthesis and characterization of mesoporous silica nanoparticles using ionic liquids as a template, *J. Phys.: Conf. Ser.*, 2018, **1123**, 012068.

32 A. K. Sutanto, Y. Xing, T. Ding, Z. Wang, K. Sun, D. Mo, J. Zhang and K. Cai, Hybrid mesoporous nanoparticles with highly integrated polydopamine for pH-responsive membrane permeation and drug delivery, *Colloid Interface Sci. Commun.*, 2021, **41**, 100385.

33 T. P. Nguyen, P. Hesemann, T. M. Linh Tran and J. J. E. Moreau, Nanostructured polysilsesquioxanes bearing amine and ammonium groups by micelle templating using anionic surfactants, *J. Mater. Chem.*, 2010, **20**(19), 3910–3917.

34 U. D. Thach, P. Trens, B. Prelot, J. Zajac and P. Hesemann, Tuning the Interfacial Properties of Mesoporous Ionosilicas: Effect of Cationic Precursor and Counter Anion, *J. Phys. Chem. C*, 2016, **120**(48), 27412–27421.

35 H. Wu, P. Hesemann, P. Trens, G. Silly, F. Salles and J. Zajac, Ionosilica-based anion exchangers for low-temperature thermochemical storage of energy under mild conditions of adsorbent regeneration and saturation, *Chem. Eng. J.*, 2020, **398**, 125634.

36 A. D. Rodrigues, M. Jacob, V. Gauchou, J.-O. Durand, P. Trens, B. Prelot and P. Hesemann, Controlled synthesis and osmotic properties of ionosilica nanoparticles, *Microporous Mesoporous Mater.*, 2021, **310**, 110644.

37 A. D. Rodrigues, M. Jacob, V. Gauchou, J. O. Durand, P. Trens and P. Hesemann, Quaternary Ammonium-Based Ionosilica Hydrogels as Draw Solutes in Forward Osmosis, *Molecules*, 2020, **25**(24), 5987.

38 U. D. Thach, B. Prelot, S. Pellet-Rostaing, J. Zajac and P. Hesemann, Surface Properties and Chemical Constitution as Crucial Parameters for the Sorption Properties of Ionosilicas: The Case of Chromate Adsorption, *ACS Appl. Nano Mater.*, 2018, **1**(5), 2076–2087.

39 R. Bouchal, I. Miletto, U. D. Thach, B. Prelot, G. Berlier and P. Hesemann, Ionosilicas as efficient adsorbents for the separation of diclofenac and sulindac from aqueous media, *New J. Chem.*, 2016, **40**(9), 7620–7626.

40 R. Bouchal, M. Daurat, M. Gary-Bobo, A. Da Silva, L. Lesaffre, D. Aggad, A. Godefroy, P. Dieudonne, C. Charnay, J. O. Durand and P. Hesemann, Biocompatible Periodic Mesoporous Ionosilica Nanoparticles with Ammonium Walls: Application to Drug Delivery, *ACS Appl. Mater. Interfaces*, 2017, **9**(37), 32018–32025.

41 M. Daurat, S. Rahmani, R. Bouchal, A. Akrout, J. Budimir, C. Nguyen, C. Charnay, Y. Guari, S. Richeter, L. Raehm, N. Bettache, M. Gary-Bobo, J. O. Durand and P. Hesemann, Organosilica Nanoparticles for Gemcitabine Monophosphate Delivery in Cancer Cells, *ChemNanoMat*, 2019, **5**(7), 888–896.

42 B. Mezghrani, L. M. A. Ali, S. Richeter, J. O. Durand, P. Hesemann and N. Bettache, Periodic Mesoporous Ionosilica Nanoparticles for Green Light Photodynamic Therapy and Photochemical Internalization of siRNA, *ACS Appl. Mater. Interfaces*, 2021, **13**(25), 29325–29339.

43 N. Abdou, P. Landois, N. Brun, B. Alonso, A. Taubert, P. Hesemann and A. Mehdi, Ionic Guest in Ionic Host: Ionosilica Ionogel Composites via Ionic Liquid Confinement in Ionosilica Supports, *Mater. Chem. Front.*, 2022, **6**, 939–947.

44 M.-A. Neouze, J. Le Bideau, P. Gaveau, S. Bellayer and A. Vioux, Ionogels, New Materials Arising from the Confinement of Ionic Liquids within Silica-Derived Networks, *Chem. Mater.*, 2006, **18**(17), 3931–3936.

45 R. Goebel, P. Hesemann, J. Weber, E. Moller, A. Friedrich, S. Beuermann and A. Taubert, Surprisingly high, bulk liquid-like mobility of silica-confined ionic liquids, *Phys. Chem. Chem. Phys.*, 2009, **11**(19), 3653–3662.

46 S. Brunauer, P. H. Emmett and E. Teller, Adsorption of Gases in Multimolecular Layers, *J. Am. Chem. Soc.*, 1938, **60**(2), 309–319.

47 E. P. Barrett, L. G. Joyner and P. P. Halenda, The Determination of Pore Volume and Area Distributions in Porous Substances. I. Computations from Nitrogen Isotherms, *J. Am. Chem. Soc.*, 1951, **73**(1), 373–380.

48 L. Viau, M. A. Neouze, C. Biolley, S. Volland, D. Brevet, P. Gaveau, P. Dieudonne, A. Galarneau and A. Vioux, Ionic Liquid Mediated Sol-Gel Synthesis in the Presence of Water or Formic Acid: Which Synthesis for Which Material?, *Chem. Mater.*, 2012, **24**(16), 3128–3134.

49 W. D. Harkins and G. Jura, Surfaces of solids XIII A vapor adsorption method for the determination of the area of a solid without the assumption of a molecular area,

and the areas occupied by nitrogen and other molecules on the surface of a solid, *J. Am. Chem. Soc.*, 1944, **66**, 1366–1373.

50 H. D. Burrows and J. S. Frontmatter, *Pure Appl. Chem.*, 2015, **87**, i–iv.

51 G. W. Scherer, S. Calas and R. Sempéré, Adsorption in Sparse Networks: II. Silica Aerogels, *J. Colloid Interface Sci.*, 1998, **202**(2), 411–416.

52 J. N. A. Canongia Lopes and A. A. H. Padua, Nanostructural Organization in Ionic Liquids, *J. Phys. Chem. B*, 2006, **110**(7), 3330–3335.

53 M. N. Garaga, M. Nayeri and A. Martinelli, Effect of the alkyl chain length in 1-alkyl-3-methylimidazolium ionic liquids on inter-molecular interactions and rotational dynamics A combined vibrational and NMR spectroscopic study, *J. Mol. Liq.*, 2015, **210**, 169–177.

